Design and Analysis of a Hybrid Permanent Magnet Assisted Synchronous Reluctance Motor Considering Magnetic Saliency and PM Usage

Wenye Wu, *Student Member, IEEE*, Xiaoyong Zhu, *Member, IEEE*, Li Quan, Yi Du, Zixuan Xiang, and Xuhui Zhu

Abstract—This paper proposes a new hybrid permanent magnet (PM)-assisted synchronous reluctance motor, where two types of PM materials of rare-earth PMs and ferrite PMs are employed in its rotor. To reduce the usage of rare-earth materials, a hierarchical design method is adopted in its rotor design, in which the design is divided into two levels: saliency ratio design level and PM usage design level. In saliency ratio design level, proper flux barrier dimensions are confirmed based on the principle of reluctance torque maximization. In PM usage design level, the optimal magnet ratio is first determined according to the relationship of main flux and leakage flux. Then, a tradeoff design is conducted to seek the superior combination of low torque ripple, high efficiency, and high power factor. Finally, for the purpose of validation, the electromagnetic performances of the new designed motor are investigated, including torque characteristics and antidemagnetization capabilities of ferrite.

Index Terms—Hybrid PM, hierarchical method, PM-assisted motor, saliency ratio, PM usage.

I. Introduction

PERMANENT magnet synchronous machines (PMSMs) have been appreciated and widely employed in various applications owing to the high energy density of rare-earth materials. However, in recent years, the cost of rare-earth permanent magnet (PM) has experienced drastic fluctuations, which brings great challenges to the motors that mainly relied on vast rare-earth permanent magnet to retain strong output capabilities [1]–[3].

To obtain a low cost design in PMSMs, making full use of reluctance torque generated by the rotor saliency is a key technique. This technique has been well implemented in synchronous reluctance motors [4], [5]. And yet, the drawback of low power factor limits its far-reaching development in industrial applications [5]. In response, a kind of PM-assisted synchronous reluctance motor (PM-assisted motor) has been

proposed and thoroughly studied by many authors [6]–[8]. Due to a large saliency, this kind of motor reveals a relatively low desire for the high energy PMs with respect to PMSMs. Therefore, the rare-earth-free PM-assisted synchronous reluctance motors using such as ferrite have been aroused considerable attention. Studies have shown that, by both using PM torque and reluctance torque component, the torque density, power factor and efficiency of the motor can be enhanced considerably in comparison with reluctance motors [9]. Whereas the irreversible demagnetization causing by the relatively low remanence and coercivity for ferrite PMs is still a headache when flux-weakening condition is involved [10], [11].

In this paper, by adding a less amount of rare-earth PMs to ferrite PM-assisted synchronous reluctance motor, a new type of hybrid PM-assisted synchronous reluctance motor is proposed, where the low-cost advantage of ferrite material is retained. Meanwhile, the added flux linkage from rare-earth PMs is expected to provide a protective effect on ferrite PMs for its reversible demagnetization. Since multiple flux barriers and multiple excitation sources are incorporated in its rotor, a more complex rotor structure produces more design degrees of freedom. Thus, it is a great challenge to design such a hybrid PM-assisted synchronous reluctance motor both with reasonable rotor saliency and proper PM usage. To meet this challenge, a hierarchical design method is adopted to divide the rotor design into two levels, including saliency ratio design level and PM usage design level. As a result, classified design objectives can be respectively realized in each level. In saliency ratio design level, the reasonable flux barrier dimensions are optimized. And in PM usage design level, the optimal magnet ratio is determined and the low torque ripple, high efficiency and high power factor are also obtained. Finally, the involved electromagnetic performances of the new designed motor are analyzed to verify the feasibility of the design method.

II. Motor Topology and Magnetic Circuit

A. Motor Topology

The configuration of the proposed motor and its details are shown in Fig. 1, and its main design specifications and design requirements are summarized in Table I. In this motor, distributed windings are adopted to have a high torque capability and a low torque ripple. To profoundly utilize reluctance torque, three layers of flux barriers are stacked in its rotor radial direction,
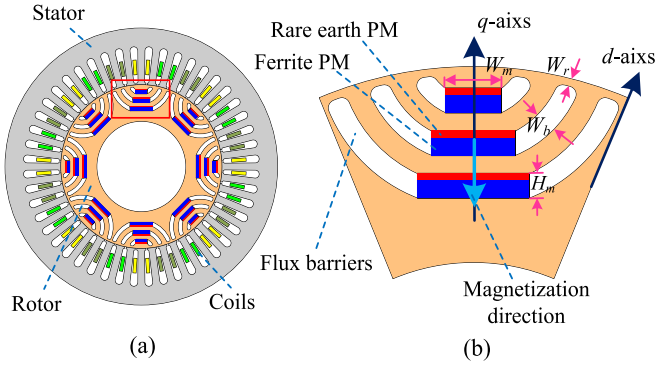
Fig. 1.   Motor configurations. (a) Whole motor. (b) Details and parameters.

TABLE I
MAIN DESIGN SPECIFICATIONS AND DESIGN OBJECTIVES

| Parameters	Values	Parameters	Values
Outside stator diameter	195 mm	Rated power	5.0 kW
Inner stator diameter	116 mm	Rated speed	1200 rpm
Stack length	65 mm	Rated torque	40 Nm
Outside rotor diameter	115 mm	Peak torque	80 Nm
Number of slots/pole	48/8	Rate current density	6.5 A/mm^2
Number of turns	16	Peak current density	13.0 A/mm^2
Parallel circuits	1	Efficiency η	$\geq$90%
Coil fill factor	65%	Power factor P_F	$\geq$73%
DC voltage	78 V	Torque ripple T_R	$\leq$6.0 Nm
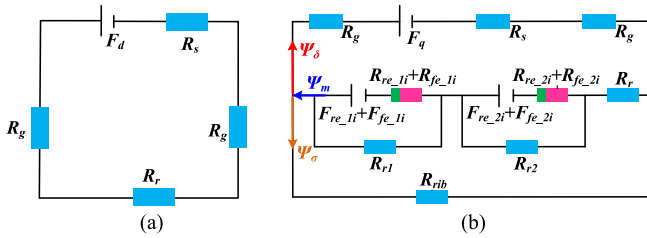
Fig. 2.   Equivalent magnetic circuits. (a) d-axis. (b) q-axis.

making it possible to provide a large design freedom for saliency ratio. The special feature of the rotor is that two types of PMs such as rare earth (NdFeB) and ferrite (Y30) are inset in its flux barriers, where the two rectangular PM pieces in each barrier are spliced together, forming a serial magnetic circuit. It is noted that the magnetization direction of both of the PMs is opposite to q-axis. Thus, compared with the reluctance motor, the added PM flux linkage not only offsets a part of flux linkage of stator excitation, so as to increases the power factor of the motor, but also yields an additional contribution to the electromagnetic torque.

B. Magnetic Circuit Characteristics

Fig. 2 shows the equivalent magnetic circuits of d-axis and q-axis of the proposed motor. Here, R_s, R_r, R_g, R_{rib}, R_{re} and R_{fe} are the reluctance of stator iron, rotor iron, air gap, ribs, rare-earth PMs and ferrite PMs, respectively. $Rre\_1i + Rfe\_1i$ and $Rre\_2i + Rfe\_2i$ respectively represent the total reluctance of three layers of PMs in two adjacent magnet poles. Obviously, in d-axis, due to a high magnetic permeability of stator and rotor

TABLE II
ARRANGEMENT OF DESIGN LEVEL

Level	Design objectives	Key design variables
Magnetic saliency design level	Magnetic saliency	Width of barriers W_b
	Reluctance torque	Width of ribs W_r
PM usage design level	Efficiency Power factor	Magnet ratio k PM width
	Torque ripple	W_m PM thickness H_m

core, the potential drop for magnetomotive force of F_d generated by stator reaction force is mainly located in the air gap, which is generally considered to be negligible. However, in q-axis, the flux from stator have to overcome a larger reluctance caused by multiple flux barriers, resulting in a corresponding enormous potential drop for F_q. Furthermore, since the magnetomotive force of F_{re} and F_{fe} generated by rare-earth PMs and ferrite PMs are contrary to F_q (where the total magnetomotive force from three layers of PMs in two adjacent magnet poles are respectively represented by $Rre\_1i + Rfe\_1i$ and $Rre\_2i + Rfe\_2i$), the magnetic potential of q-axis is consequently further reduced. In summary, the flux barrier design in the rotor facilitates the crossing of the magnetic field in d-axis rather than its q-axis.

In addition, the flux ψ_m from the two types of PMs are divided into main flux ψ_δ and leakage flux ψ_σ. In particular, the ψ_δ moves to stator to offset the stator flux linkage and produce an assisted torque. As for the ψ_σ, which tends to saturate the ribs at the top of barrier tips, indirectly decreasing the permeability of q-axis, and resulting in a reduction of the magnetizing current.

III. HIERARCHICAL DESIGN

Based on above analysis of the characteristics of the proposed motor, two feasible schemes to reduce the design cost of the motor can be drawn. One is to make use of reluctance torque, and the other is to reasonably design the usage of rare-earth materials. Generally, the reluctance torque is depended on the level of saliency ratio of rotor, and the usage of PMs is decided by the proportion of the two types of PMs and the quantity of total PMs. Followed by this two aims, a more complex rotor structure and more design degrees of freedom will be formed. Thus, in this motor, the influences of design objectives may even conflict with each other. For example, the increase of saliency ratio is beneficial to the increase of reluctance torque, but an excessive increase will result in the deterioration on mechanical properties, and it also causes a negative effect on the torque ripple. Moreover, an increase in the amount of rare earth PMs can raise motor power factor and torque output, but it causes a sharp increase in manufacture cost and an excessive saturation in its rotor. Obviously, a multi-dimensional optimization is very complicated and time-consuming, sometimes even non-convergent when all design objectives are considered simultaneously [12], [13]. Therefore, a hierarchical design method is proposed to its rotor design, the design process is divided into two levels, including magnetic saliency design level and PM usage design level, respectively. Specific design arrangement and design variables are shown is Table II.

IV. MAGNETIC SALIENCY DESIGN LEVEL

A. Condition for PM-assisted Motor

Generally, the basic torque characteristics of an interior PM motor can be expressed by the following equation in the *d–q* axis frame.

$$T = P[\psi_m + (L_d - L_q)i_d]i_q \tag{1}$$

Where *T* is the output torque, *P* is the rotor pole pair, L_d, L_q, I_d and I_q are the *d*-axis inductance, *q*-axis inductance, *d*-axis current and *q*-axis current, respectively.

It is clear that, the torque production in an interior PM motor combines two components, a magnet torque component resulting from the presence of magnets in the rotor, and a reluctance torque component resulting from magnetic saliency of rotor structure. The relative proportion of the PM torque and reluctance torque in motor design is determined by how much magnet flux linkage and how much magnetic saliency are incorporated into the motor. To clear this matter, the relationship between saliency and torque ratio are discussed through a series of derivation.

Here, in order to generate maximum torque, a maximum current from the inverter is defined as $I_{\max}$. Hence, the i_d and i_q can be defined as follows

$$i_d = I_{\max}\cos\beta \tag{2}$$

$$i_q = I_{\max}\sin\beta. \tag{3}$$

Where the β is the angle of *d*-axis and current vector of I_{max}. The saliency ratio ρ, is defined as

$$\rho = \frac{L_d}{L_q}. \tag{4}$$

By substituting the i_d and i_q into torque equation of (1), the torque *T* can be expressed as a function of the current angle β. And then, taking the derivative of the torque with respect to β, and putting the result to zero. It is possible to get the value of β that achieves the maximum torque. It is given as follows

$$\cos\beta = \frac{-\psi_m + \sqrt{\psi_m^2 + 8I_{\max}^2(\rho-1)^2 L_q^2}}{4(\rho-1)L_q I_{\max}}. \tag{5}$$

Besides, the ratio of magnet torque T_m and reluctance torque T_r is defined as a value of *f*, that is

$$f = \frac{T_m}{T_r} = \frac{\psi_m i_d}{(L_d - L_q)i_d i_q}. \tag{6}$$

Therefore, when the maximum torque is obtained, the above equation can be expressed as following condition

$$\frac{\sqrt{2 + f}}{f(\rho - 1)} = \frac{i_{\max}L_q}{\psi_m}. \tag{7}$$

If L_q is chosen as its optimum value, namely, the maximum current is enough to offset permanent magnet flux linkage completely. Hence, a relationship between *f* and ρ can be given below
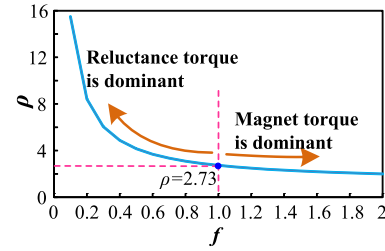
$$\rho = \frac{\sqrt{2 + f}}{f} + 1. \tag{8}$$

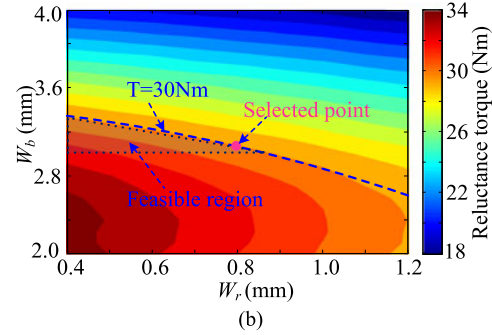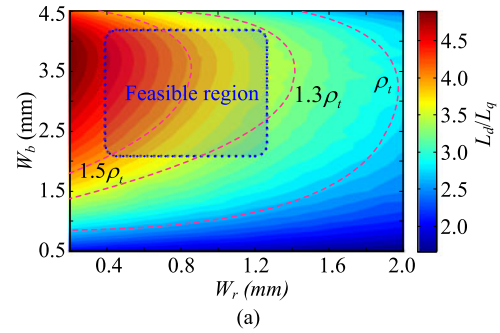Fig. 3. Relationship between *f* and ρ.

Fig. 4. Flux barrier design. (a) The relationship of saliency ratio versus W_b and W_r. (b) The relationship of reluctance torque versus W_b and W_r.

Fig. 3 shows the plot of (8), which indicates the relationship of motor saliency ratio and the relative proportion of magnet torque and reluctance torque. If the case of $f < 1$ (i.e., the reluctance torque is a dominant component) is identified as PM-assisted motor, it can be believed that the prerequisite for a PM-assisted motor is that the saliency ratio must be greater than the threshold value of 2.73. In the following discussion, this value can be called ρ_t.

B. Flux Barrier Design

Based on above analysis, the saliency ratio condition of achieving PM-assisted motors has been determined. In this section, the discussion will deal with the selection of flux barrier parameters based on the threshold value of ρ_t. It can be known from the magnetic circuit analysis that the width of flux barriers of W_b and width of the ribs of W_r at the top of flux barrier tips have the most effect on saliency ratio. Thus this two parameters are selected as design variables in this design level. Considering the design space of rotor and the mechanical strength restrictions, the variation ranges of W_b and W_r are set as 0.5 mm to 4.5 mm and 0.2 mm to 2.0 mm, respectively. The relationship of saliency ratio versus W_b and W_r are shown in Fig. 4(a). It
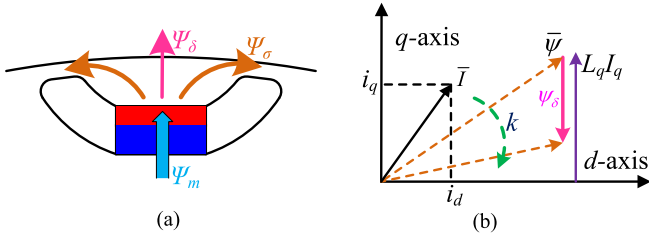
Fig. 5. The selection principles of PM flux linkage. (a) The path of main flux and leakage flux. (b) The offset effect of PM flux.
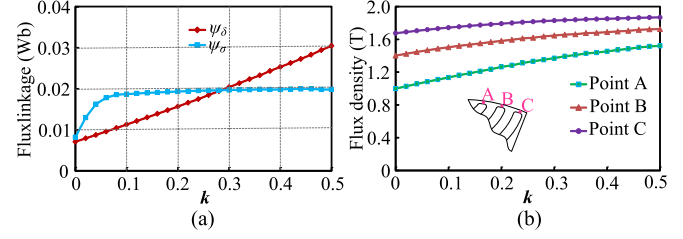

Fig. 6. Selection of PM flux linkage. (a) The variation of main flux linkage and leakage flux linkage versus k. (b) The saturation level of the ribs versus k.

can be observed that a lower W_r and a thicker W_b result in a higher saliency ratio. And the vast majority of the region can meet the threshold value of ρ_t. In this case, the region higher than 1.3 ρ_t is considered to be available. Moreover, considering that the negative influence caused by saturation may be emerged in a too thick flux barrier, the preliminary selection of feasible region is depicted by a shaded region.

In order to further confirm the W_b and W_r, the relationship of reluctance torque versus W_b and W_r are investigated according to previous choice. And its results are shown in Fig. 4(b). Since the dominant torque is from reluctance torque, the reluctance torque is considered to be designed as high as possible. Here, based on the design requirements, the reluctance torque is intended to be higher than three-quarter of rated torque (40 Nm). As a result, the final feasible region of W_b and W_r is obtained and marked in shade region. It should be pointed out that a narrow rib may not be able to meet the mechanical requirements. Thus, finally, the W_b and W_r are confirmed as 3.2 mm and 0.8 mm, respectively.

V. PM USAGE DESIGN LEVEL

A. PM Flux Linkage Selection

Fig. 5 shows the selection principles of PM flux in a PM-assisted motor. From Fig. 5(a), it illustrates that the flux from PMs are divided into two paths on the rotor island bordered by flux barriers and air gap. In particular, the leakage flux ψ_σ pass through the ribs to link to the PMs in adjacent magnet poles, forming a closed magnetic circuit in its rotor. The quantity of ψ_σ determines the degree of saturation of the ribs. While for the main flux linkage of ψ_δ, which flows into stator to offset the stator flux of $L_q I_q$, and tends to rotate the flux linkage vector of $\bar{\psi}$ away from the current vector of $\bar{I}$, resulting in an increase of power factor, as shown in Fig. 5(b). The rotated angle of $\bar{\psi}$ is determined by the level of ψ_δ. And the level of ψ_δ is in turn related to magnet proportion of rare earth and ferrite. Thus, the proportion of the ψ_σ and ψ_δ should be a key consideration in this motor design.

In order to simplify the analysis, a value of k is employed to define the magnet ratio of rare-earth PMs and ferrite PMs. Which is

$$k = \frac{V_{re}}{V_{re} + V_{fe}}. \tag{9}$$

Where V_{re} and V_{fe} are the total volume of rare-earth PMs and ferrite PMs. Because the two PMs have the same width, the

magnet ratio can also be defined by follow equation (10)

$$k = \frac{H_{re}}{H_{re} + H_{fe}} \tag{10}$$

Here, the H_{re} and H_{fe} are the thickness of the rare-earth PMs and ferrite PMs.

The variations of main flux and leakage flux linkage versus k are shown in Fig. 6(a). It can be observed that the main flux of ψ_δ possesses a growing trend with the increase of k, whereas the leakage flux of ψ_δ reaches its saturation at a very low k value and then retains the same with the increase of k. More remarkably, only when k is greater than 0.3, the ψ_δ begins to higher than ψ_σ. That is, at least 30% of rare earth usage is needed to realize main flux greater than leakage flux in this hybrid PM-assisted motor. Fig. 6(b) shows the saturation level of the ribs owing to leakage flux. It can be found, with the increase of k, the flux densities of all of the three point of A, B and C present rising trends. In particular, the point C reaches its saturation threshold (1.8 T) when k is greater than 0.3. It means the usage of rare-earth PMs with $k = 0.3$ is enough to saturate the ribs, so as to block more flux in the q-axis. Thus, the optimal magnet ratio of rare-earth PMs and ferrite PMs is determined to be 0.3.

B. Tradeoff Design

After the optimal magnet ratio of rare-earth PMs and ferrite PMs is determined, to meet design requirement, the thickness and width of PMs need to be addressed as well. Here, the thickness of PMs in each layer of flux barriers is specified as an equal variable, while its width is set as an arithmetic progression from first layer to third layer with a common difference of 3 mm. In general, response surface method is considered as an effective approach to clarify the complex relationship between design variables and design objectives. Thus, the response surface method is adopted in this motor design to ravel out the interactive influences of the three design objectives with the variations of design variables of PM thickness (H_m) and PM width (W_m) in first layer, which is shown in Fig. 7. It can be observed that there are some conflicts between the three design objectives. For instance, with the increase of H_m, a higher power factor is obtained, but its efficiency shows a declined trend. Thus, a tradeoff selection should be conducted to further determine the optimal dosage of permanent magnets.

Fig. 8 shows the tradeoff design of the three design objectives. Here, the different design points are located in a three-dimensional space constructed by the three design objectives. Based on the design requirement mentioned in Table I, an
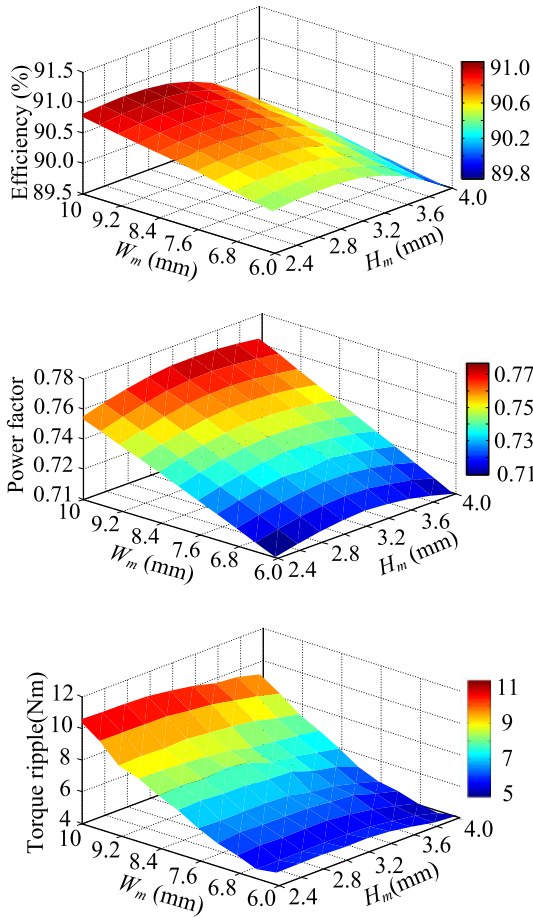
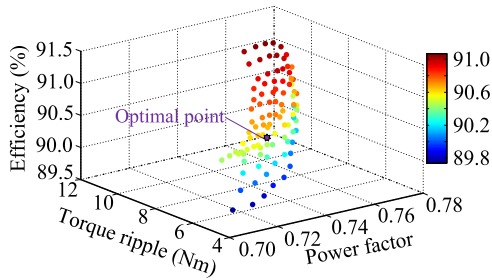Fig. 7. The response surface analysis of different design objectives.

Fig. 8. The tradeoff design based on the three design objectives.

optimal point that balanced each objective is finally determined. Then the corresponding values of PM thickness and PM width are obtained. Finally, the optimization objectives and the key design variables of the new hybrid PM-assisted synchronous reluctance motors are listed in Table III.

VI. PERFORMANCES INVESTIGATION

A. Torque Analysis

The torque versus current angle characteristics of the new design motor at the rated current are presented in Fig. 9. As shown in Fig. 9(a), the reluctance torque is the dominant component of the motor and which accounts for almost three-quarters of total torque when the maximum torque is achieved, while the PM torque from rare-earth PMs and ferrite PMs exhibits a relatively

TABLE III
OPTIMIZATION RESULT OF THE HYBRID MOTOR

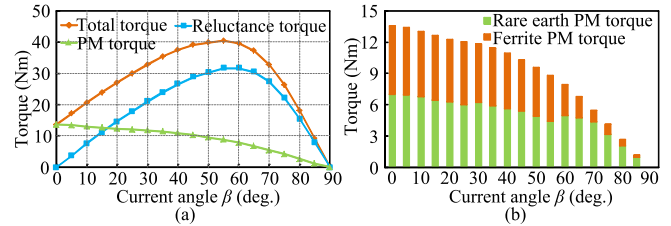| Items	Optimal value	Items	Optimal value
W_r	0.8 mm	k	0.3 mm
W_b	3.2 mm	η	90.46%
W_m	6.8 mm	P_F	0.73
H_m	3.4 mm	T_R	5.98 Nm

Fig. 9. The torque characteristics. (a) Torque components versus current angle. (b) The torque proportion of rare-earth PMs and ferrite PMs versus current angle.
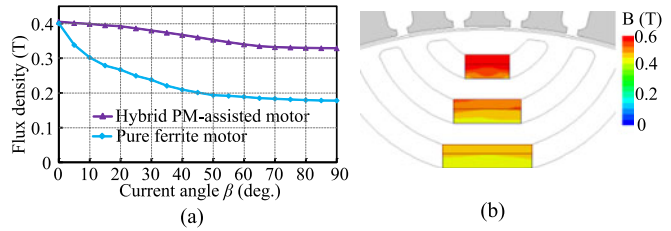

Fig. 10. Anti-demagnetization capabilities (a) the variations of minimum flux density of ferrite PMs versus β in the hybrid PM-assisted motor and a pure ferrite motor. (b) The flux density distributions of ferrite PMs under the maximum flux-weakening condition ($\beta = 90°$) in the hybrid PM-assisted motor.

low proportion of total torque. It illustrates that PMs in this motor only act an assisted role, and the usage of rare-earth PMs of NdFeB is expected to be reduced. From Fig. 9(b), it can be obtained that the rare-earth PMs and ferrite PMs produce almost equal torque component, though only 30% rare-earth PMs are contained in total PM usage. It indicates that a less amount of rare earth is sufficient for a PM-assisted synchronous reluctance motor to guarantee a high torque output.

B. Anti-Demagnetization Capabilities

Generally, the irreversible demagnetization is thought to occur when the PM's flux density is lower than the flux density of its knee point. As for ferrite PMs used in the proposed motor, this threshold value is generally supposed to be 0.2 T in 20 °C. To clarify the interaction between rare-earth PMs and ferrite PMs, simulations are carried out in this proposed hybrid PM-assisted motor and a pure ferrite PM-assisted motor underrated operation condition. As shown in Fig. 10(a), due to the protective effect of a less amount of NdFeB PMs, the ferrite operating point presents a slower declined trend with the increasing of β, and it remains above its knee point even when the demagnetizing current in q-axis reach its maximum ($\beta = 90°$). While in the pure ferrite motor, with the increase of the β, i.e., the applied current is rotated from d-axis to q-axis, the flux density in ferrite PMs falls below its knee point as the current angle is greater than 50°. It means that the ferrite PMs in the pure ferrite

motor will suffer from a serious irreversible demagnetization under flux-weakening operating conditions.

The flux density distributions of ferrite PMs under the maximum flux-weakening condition ($\beta = 90°$) in the less-rare-earth motor are shown in Fig. 10(b). In this case, since a part of flux from rare-earth PMs and ferrite PMs leaks through ribs and forms a closed loop circuit in its rotor. Thus the low energy ferrite PMs can be magnetized by the high energy PMs of rare earth, raising the operating point of ferrite PMs nearly up to its remanence point. Consequently, there is no demagnetization area occurs in ferrite PM's bodies.

VII. CONCLUSION

In this paper, a new hybrid PM-assisted synchronous reluctance motor with two types of PM materials of rare-earth PMs and ferrite PMs is proposed, and a hierarchical design method is adopted in it rotor design. The basic conclusions are:

By incorporating both rare-earth PM and non-rare-earth ferrite PM materials in rotor flux barriers, the proposed motor can not only offer a comparable electromagnetic performance, but also achieve a low rare-earth PM usage, which offers a competitive price advantage with the pure rare-earth motors. The proposed hierarchical design method is verified to be effective in the motor design, especially for the motor with complex flux barriers and multi-excitation sources.

REFERENCES

[1] K. T. Chau, C. C. Chan, and C. Liu, "Overview of permanent-magnet brushless drives for electric and hybrid electric vehicles," *IEEE Trans. Ind. Electron.*, vol. 55, no. 6, pp. 2246–2257, Jun. 2008.

[2] G. Pellegrino, T. M. Jahns, N. Bianchi, W. L. Song, and F. Cupertino, *The Rediscovery of Synchronous Reluctance and Ferrite Permanent Magnet Motors: Tutorial Course Notes*. New York, NY, USA: Springer, 2016.

[3] Z. R. Zhang, J. Dai, C. Dai, and Y. G Yan, "Design considerations of a hybrid excitation synchronous machine with magnetic shunt rotor," *IEEE Trans. Magn.*, vol. 49, no. 11, pp. 5566–5573, Nov. 2013.

[4] K. Akatsu, M. Arimitsu, and S. Wakui, "Design and control of a field intensified interior permanent magnet synchronous machine," *IEE J. Trans. Ind. Appl.*, vol. 126, no. 7, pp. 827–834, 2006.

[5] Y. S. Kim and I. H. Park, "Topology optimization of rotor in synchronous reluctance motor using level set method and shape design sensitivity," *IEEE Appl. Supercond.*, vol. 20, no. 3, pp. 1093–1096, Jun. 2010.

[6] S. Morimoto, M. Sanada, and Y. Takeda, "Performance of PM-assisted synchronous reluctance motor for high-efficiency and wide constant-power operation," *IEEE Trans. Ind. Appl.*, vol. 37, no. 5, pp. 1234–1240, Sep./Oct. 2001.

[7] E. Howard and M. J. Kamper, "Weighted factor multi-objective design optimization of a reluctance synchronous machine," *IEEE Trans. Ind. Appl.*, vol. 52, no. 3, pp. 2269–2279, May/Jun. 2016.

[8] H. Huang, Y. S. Hu, Y. Xiao, and H. Lyu, "Research of parameters and antidemagnetization of rare-earth-less permanent magnet-assisted synchronous reluctance motor," *IEEE Trans. Magn.*, vol. 51, no. 11, Nov. 2015, Art. no. 8112504.

[9] M. Obata, S. Morimoto, M. Sanada, and Y. Inoue, "Performance of PMASynRM with ferrite magnets for EV/HEV applications considering productivity," *IEEE Trans. Ind. Appl.*, vol. 50, no. 4, pp. 2427–2435, Jul./Aug. 2014.

[10] A. Vagati, B. Boazzo, P. Guglielmi, and G. Pellegrino, "Design of ferrite-assisted synchronous reluctance machines robust toward demagnetization," *IEEE Trans. Ind. Appl.*, vol. 50, no. 3, pp. 1768–1779, May/Jun. 2014.

[11] W. Y. Wu, X. Y. Zhu, L. Quan, D. Y. Fan, and Z. X. Xiang, "Characteristic analysis of a less-rare-earth hybrid PM-assisted synchronous reluctance motor for EVs application," *AIP Adv.*, vol. 7, no. 5, 2017, Art. no. 056648.

[12] Z. X. Xiang, X. Y. Zhu, L. Quan, Y. Du, C. Zhang, and D. Y. Fan, "Multi-level design optimization and operation of a brushless double mechanical port flux-switching permanent-magnet motor," *IEEE Trans. Ind. Electron.*, vol. 63, no. 10, pp. 6042–6054, Oct. 2016.

[13] X. Y. Zhu, Z. X. Xiang, C. Zhang, L. Quan, Y. Du, and W. W. Gu, "Co-reduction of torque ripple for outer rotor flux-switching PM motor using systematic multi-level design and control schemes," *IEEE Trans. Ind. Electron.*, vol. 64, no. 2, pp. 1102–1112, Feb. 2017.